Spatial and Energy Distribution of Topological Edge States in Single Bi(111) Bilayer

Fang Yang,[1] Lin Miao,[1] Z. F. Wang,[2] Meng-Yu Yao,[1] Fengfeng Zhu,[1] Y. R. Song,[1] Mei-Xiao Wang,[1] Jin-Peng Xu,[1] Alexei V. Fedorov,[3] Z. Sun,[4] G. B. Zhang,[4] Canhua Liu,[1] Feng Liu,[2,*] Dong Qian,[1,†] C. L. Gao,[1,‡] and Jin-Feng Jia[1]

[1]*Key Laboratory of Artificial Structures and Quantum Control (Ministry of Education). Department of Physics, Shanghai Jiao Tong University, 800 Dong Chuan Road, Shanghai 200240, China*

[2]*Department of Materials Science Engineering, University of Utah, Salt Lake City, Utah 84112, USA*

[3]*Advanced Light Source, Lawrence Berkeley National Laboratory, Berkeley, California 94305, USA*

[4]*National Synchrotron Radiation Laboratory, University of Science and Technology of China, Hefei, 230026, China*

(Received 26 February 2012; published 5 July 2012)

By combining scanning tunneling microscopy and spectroscopy, angle-resolved photoemission spectroscopy, and density functional theory band calculations, we directly observe and resolve the one-dimensional edge states of single bilayer (BL) Bi(111) islands on clean Bi_2Te_3 and Bi(111)-covered Bi_2Te_3 substrates. The edge states are localized in the vicinity of step edges having an ~2 nm wide spatial distribution in real space and reside in the energy gap of the Bi(111) BL. Our results demonstrate the existence of nontrivial topological edge states of single Bi(111) bilayer as a two-dimensional topological insulator.

DOI: 10.1103/PhysRevLett.109.016801 PACS numbers: 73.20.−r

Topological insulators (TIs)—a newly discovered quantum class of materials with topological order [1–7]—have attracted intensive studies in last five years due to their unique quantum properties as proposed by theorists, such as magnetic monopole [8], Majorana fermions [9], anomalous quantum Hall effect [10], and spin related novel phenomena [11,12]. Holding charge excitation gaps in the bulk, TIs are characterized by metallic states in the onedimensional (1D) edges [twodimensional (2D) TI] or 2D surfaces [threedimensional (3D) TI]. In these metallic channels, opposite flowing charge currents are locked to the opposite spins. For spin transport, 2D TI can be advantageous over 3D TI because electrons can only move along two directions in a 2D TI. So far, however, only one 2D TI system—HgTe/CdTe quantum well—has been theoretically proposed [1] and experimentally demonstrated [2]. Several other 2D TIs are proposed, and one system that has possibly drawn the most attention is ultrathin Bi(111) films [13–16]. Very recently, single bilayer Bi(111) has been grown on Bi_2Te_3 substrate showing band structures indicative of 2D TI properties [17,18]. Unfortunately, unlike 3D TIs, it is impossible to measure the dispersion relations of edge states of 2D TIs in momentum space by angle-resolved photoemission spectroscopy (ARPES). To our best knowledge, no observation of Bi(111) edge states has been reported.

In this Letter, using real-space resolution of scanning tunneling microscopy (STM) and scanning tunneling spectroscopy (STS), we directly observe and resolve the edge states of single (bilayer) BL Bi(111) islands, in both real and energy space, which are grown on clean Bi_2Te_3 and Bi(111)-covered Bi_2Te_3 substrates. In real space, the edge states display an ~2 nm wide spatial distribution next to the island step edge, as consistently shown by both STS and first principle calculations. In energy space, by comparing ARPES spectra and density functional theory (DFT) band structures, the energy position of the observed edge states was found to lie inside the energy gap of the Bi(111) BL on both substrates. Our results indicate that the observed edge states are closely related to the 2D topological properties of Bi(111).

The experiments were carried out in ultrahigh vacuum (UHV) with a base pressure better than 1×10^{-10} Torr. 40 QL Bi_2Te_3(111) films were grown on Si(111)-7 × 7 substrate [19,20]. Bi(111) films were grown on Bi_2Te_3 films at 200 K to reduce the possible intermixing of Bi and Te. STM/STS measurements were carried out at 4.2 K. ARPES measurements were performed with a helium discharge lamp (HeI 21.2 eV) and 28–60 eV photons in advanced light source (ALS) beam line 12.0.1 with energy resolution better than 25 meV and angular resolution better than 0.02 $Å^{-1}$ at 100 K and 15 K using Scienta analyzers. First-principles DFT calculations were carried out in the framework of the Perdew-Burke-Ernzerhof-type generalized gradient proximation using the VASP package [21]. The lattice parameters of the substrate were taken from experiments ($a = 4.386$ Å for Bi_2Te_3), and the Bi bilayer is strained to match the substrate lattice parameter. All calculations were performed with a plane-wave cutoff of 600 eV on an $11 \times 11 \times 1$ Monkhorst-Pack k-point mesh. The substrate is modeled by a slab of six quintuple-layer (QL) Bi_2Te_3 and the vacuum layers are over 20 Å to ensure decoupling between neighboring slabs. During structural relaxation, atoms in the lower four QL substrate are fixed in their respective bulk positions, and the Bi overlayer and upper 2 QL of substrate are allowed to relax until the atomic forces are smaller than 0.01 eV/Å.

Bismuth grows on Bi_2Te_3 in the layer-by-layer mode with a minimum unit of one BL. The Bi(111) film grows first into individual triangular islands for coverage less than 0.5 BL [Fig. 1(a)] and then the islands coalesce into a continuous BL film with trianglelike holes as the Bi coverage increases [Fig. 1(b)]. The second BL Bi(111) islands grow after the first BL is almost completed [Fig. 1(c)]. Both the first and second BL Bi(111) films have the hexagonal lattice structure [see inset of Fig. 1(a)] with the same lattice constant of Bi_2Te_3. Sharp and straight edges can be found for the first and second BL Bi(111) islands without any reconstruction at the step edge. All the following STS studies concentrate only on those sharp edges to exclude the possible chemical and/or electrical interference at the meandering step edges.

Figure 2 presents STS maps of 1 BL Bi(111) islands near the step edges on the clean Bi_2Te_3 (1 BL/Bi_2Te_3 step) and 1 BL Bi-covered Bi_2Te_3 substrate (1 BL/Bi-Bi_2Te_3 step). The topography of 1 BL/Bi_2Te_3 step is shown in Fig. 2(a) with Bi in the upper terrace and Bi_2Te_3 in the lower terrace. Figure 2(b) shows the real-space STS mapping and Fig. 2(c) shows the bias voltage dependence of the edge states measured perpendicular to the step edge as marked by the blue arrowed line in Fig. 2(a). The red dashed lines mark the approximate position of the step edge in Figs. 2(a)–2(c). Sharp STS features were observed next to the step edge, as shown by the STS mapping in Fig. 2(b) ($V_{bias} = 283$ mV) and spectra in Fig. 2(c). The edge states are visible in the energy range between +136 mV to +370 mV indicated by red dots in Fig. 2(c). Their peak positions are essentially energy independent within this energy window, which excludes the possibility of their standing wave origin. Near the dominant peaks marked as red dots in Fig. 2(c), there are some weak and broad dispersive peaks which are energy dependent coming from the electronic standing waves (interference) on the surface.

The edge states were observed at the 1 BL/Bi-Bi_2Te_3 step as well, as shown in Figs. 2(d)–2(f), which correspond to Figs. 2(a)–2(c), respectively. The Bi(111) island edge states are qualitatively similar on two substrates but with some notable quantitative differences. The 1 BL/Bi-Bi_2Te_3 edge state appears in a narrower energy window from +295 mV to +377 mV than the 1 BL/Bi_2Te_3 edge state from +136 mV to +370 mV. This is because the band gap of 1 BL/Bi-Bi_2Te_3 is smaller than 1 BL/Bi-Bi_2Te_3 [comparing Fig. 4(d) to 4(a) below]. Also, the 1 BL/Bi-Bi_2Te_3 edge state has a lower intensity than the 1 BL/Bi_2Te_3 edge state. This is possibly related to the larger background density variation from the standing wave originated from quantum interference of the scattered electrons on the complete first Bi(111) BL [Bi(111) surface] as marked by the blue dots in Fig. 2(f). This

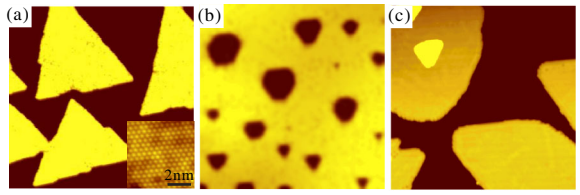

FIG. 1 (color online). STM images of (a) 0.5 BL (90 nm × 90 nm), (b) 0.8 BL (46 nm × 46 nm), and (c) 1.5 BLs (64 nm × 64 nm) Bi(111) on 40 QL Bi_2Te_3. The inset of (a) shows the atomically resolved image of 1 BL Bi(111) on Bi_2Te_3.

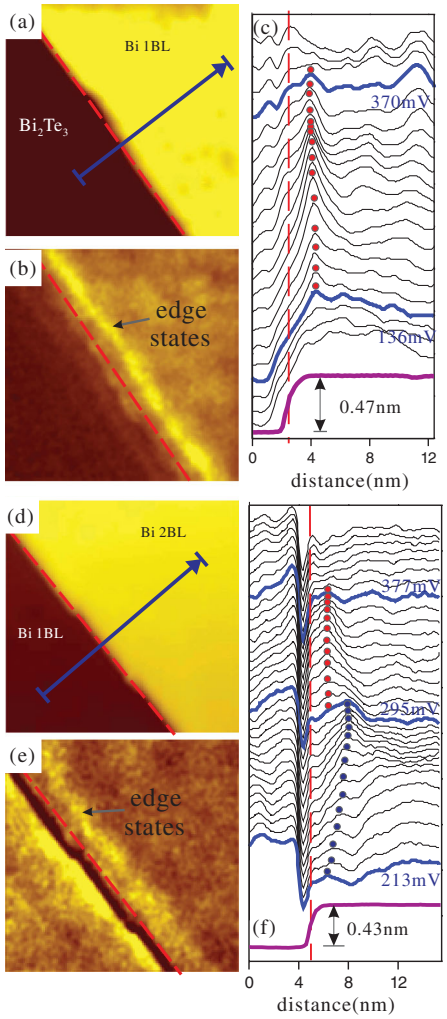

FIG. 2 (color). (a) STM image of 1 BL/Bi_2Te_3 island showing the step edge between them ($V_{sample} = 0.75$ V, $I = 245$ pA). (b) STS map at +283 mV corresponding to (a). (c) Profiles of STS maps together with the STM line scan along the blue arrowed line in (a). All neighboring STS profiles have the same bias difference of 16.7 mV. (d) The STM image of a step edge between 1 BL/Bi-Bi_2Te_3 island ($V_{sample} = 1.0$ V, $I = 300$ pA). (e) STS map at +338 mV corresponding to (d). (f) Profiles of STS maps together with the STM line scan along the blue arrowed line in (d). All neighboring STS profiles have the same bias difference of 6.5 mV. The red dots mark the peak position of the edge states. The blue dots mark the peaks of surface standing waves. The red dashed lines in (a)–(f) indicate the location of step edges.

interference peak changes its position with the increasing bias voltages (dispersive). The edge states are, however, not observed in thicker films (not shown) possibly due to the strong interference pattern at the surface or due to the nearly gapless bulk states of Bi(111).

For both Bi(111) islands of 1 BL/Bi_2Te_3 and 1 BL/Bi-Bi_2Te_3, the edge state spreads over several atomic rows with an ~2 nm width in real space. It is much wider than the typical electronic edge state, arising from edge dangling bonds or atomic reconstructions, which is highly localized on the edge atoms in one or two lattices and decays exponentially away from the edge such as the edge state of graphene [22,23]. Note that the contribution of the chemical dangling bonds, even present, cannot influence the feature nanometers away from step edge. The penetration depth of the topological edge states varies from a few to a few tens of nanometers depending on their k-space dispersion that is different from material to material [15,24]. The wide spatial distribution in real space (relative to normal electronic edge state) indicates that these are likely topological edge states of 2D TIs. To further confirm this, we calculated the edge states of a freestanding Bi(111) BL nanoribbon, which is tensile strained to the lattice constant of Bi_2Te_3. The bands are plotted in Fig. 3(a), and the real-space edge state distribution is shown in Fig. 3(b). The edge state is characterized by an odd number of crossings over the Fermi surface (from 0.0 to 1.0 in **k** space) and the spin-momentum locking (the spin is perpendicular to **k**) indicating its topological nature. The width of the spatial distribution is k-point dependent ranging from ~0.7–2 nm, as shown for six k-points in Fig. 3(b). At a given energy, the experimentally measured distribution has contributions from multiple k-points, giving rise to the observed width. These results generally agree well with the previous theoretical calculations [15]. Note that the calculated gap in Fig. 3(a) is much larger than the experimental one, because

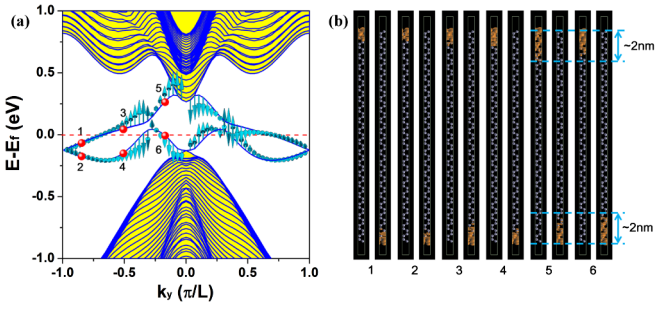

FIG. 3 (color online). (a) Band structure of the Bi(111) zigzag edge ribbon with a width of 20 unit cells. The shaded regions are the bulk states with a gap; the two solid blue lines inside the gap are edge states. The arrows denote the spin orientations of edge states indicating spin warping continuously perpendicular **k**. Here, only one edge-state spin orientation is plotted for each band. (b) Real-space charge density distribution of the edge states at different k-points as marked in (a).

it is calculated for a freestanding ribbon. When it is placed on a substrate, the gap reduces substantially, as we discuss below.

The strong k-dependence alone cannot prove the topological edge sate, because nontopological surface state can show a strong k-dependence too [25]. The 1D topological edge states are expected to be inside the bulk gap of 2D TIs [6,15]. Because the observed edge states in Fig. 2 are located above the Fermi level where no experimental data are available, we compare our STS data with the DFT band calculations. Figure 4(a) and 4(d) show the bands of top Bi(111) BL of one and two BLs of Bi on Bi_2Te_3 substrate, respectively. We note that the Dirac point in the calculated DFT band structure is not purely from the Bi_2Te_3 substrate, but a hybridized state between Bi_2Te_3 and Bi BL [17,18] as the energy of Bi BL Dirac point induced by the substrate coincides with that of Bi_2Te_3. In the ARPES experiment, due to the photoelectron escape depth (0.5–1 nm), the measured band dispersions mainly come from the top Bi BL. Figures 4(b) and 4(e) show the ARPES data laid on top of the DFT bands only from the top Bi BL. The overall agreement between ARPES spectra and DFT bands are very good except the slight shift of Fermi level, which has allowed us to extract the energy position of edge states. Note that due to the limited thickness of Bi_2Te_3 used, quantum well states are present in the calculated band [Figs. 4(a) and 4(d)], but absent in the experimental spectra in Figs. 4(b) and 4(e), taken from the Bi(111) BL on 40 QL Bi_2Te_3.

Figures 4(c) and 4(f) show the dI/dV curves of the inner terrace (wide red rectangle in the inset) and the edge-state area (narrow blue rectangle in the inset) in the island of 1 BL/Bi_2Te_3 and 1 BL/Bi-Bi_2Te_3, respectively. It has been demonstrated that the Dirac point corresponds to a dip in the dI/dV spectra due to its zero density of states [26]. Thus, we can align the dip feature in the STS spectra [Figs. 4(c) and 4(f)] to the calculated Dirac point [Figs. 4(a), 4(b), 4(d), and 4(e)], as marked by the dashed vertical blue lines. Then, we can locate the energy position of the edge states relative to the band gap position of Bi(111) BL. For the 1 BL/Bi_2Te_3 step edge [Fig. 3(c)], in the energy window from +136 mV to +370 mV, the blue curve intensity is noticeably higher than the red curve, which is exactly where the edge states are located [Fig. 2(c)]. It also agrees well with the calculated band gap (~ 76 meV) of 1 BL/Bi_2Te_3 film in Figs. 4(a) and 4(b), as marked by two dashed vertical orange lines. It is reasonable to expect that the STS attain higher contrast when STM scans over the edge state within the energy window of the band gap, where the surface electronic states are absent and the edge electronic states are highly localized within. The observed energy range of edge states is slightly larger than the band gap, possibly due to the energy extension of edge states in large k [15]. Very similar results are obtained for the 1 BL/Bi-Bi_2Te_3 edge states as shown

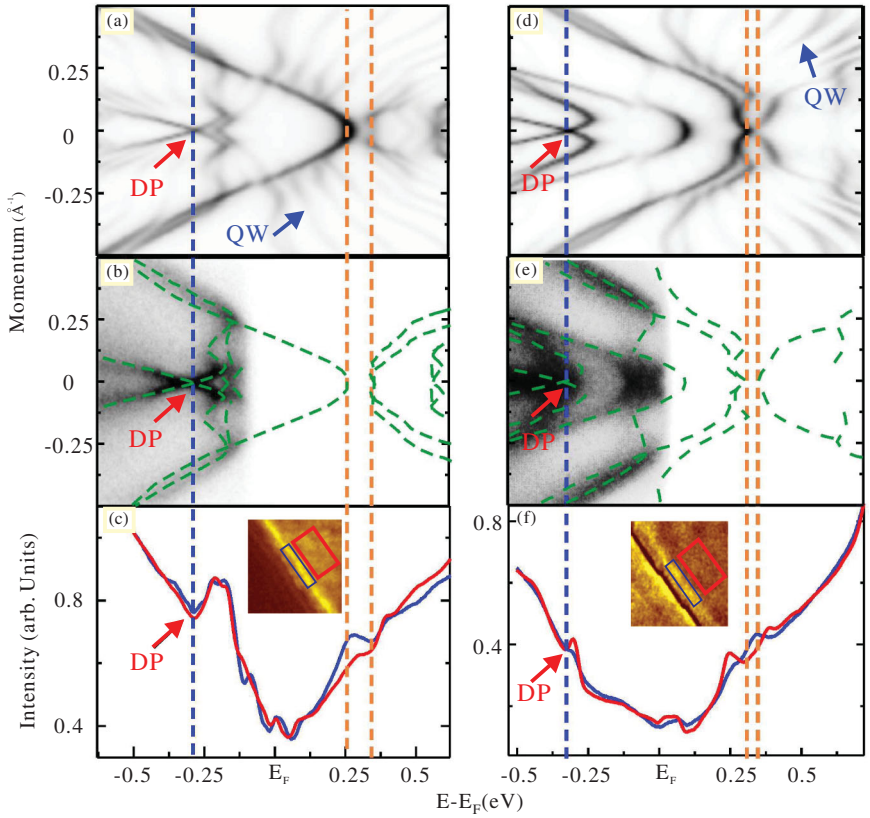

FIG. 4 (color). (a) [(d)] Calculated density of the electronic structure in the topmost Bi(111) BL of 1 BL/Bi_2Te_3 [2 BL/Bi_2Te_3] (M-Γ-M). "QW" marks the quantum well states. (b) [(e)] ARPES spectrum for 1 BL [2 BL] Bi(111) on 40 QL Bi_2Te_3 together with the surface originated bands taken from (a) [(d)]. (c) [(f)] STS of the step edge (blue) and the inner terrace (red) of 1 BL/Bi_2Te_3 [1 BL/Bi-Bi_2Te_3] island averaged over the area as marked in the inset of (c) [(f)]. The STS, ARPES, and calculated bands are aligned by the Dirac point "DP" as indicated by the blue dashed line. The orange dashed lines mark the band gap of topmost Bi BL.

in Figs. 4(d)–4(f), except with a smaller gap (~ 44 meV) and lower contrast in the energy window of +295 mV to +377 mV. The fact that edge states are observed next to the step edge with spatial distribution of several nanometers in real space and lies directly inside the 2D bulk band gaps in both cases clearly demonstrates the existence of 1D topological in-gap edge states in the Bi bilayer. Our DFT calculations also show the 1D helical spin-momentum locking property of the edge states as shown in Fig. 3(a), which is an interesting subject for future experimental study.

This work is supported by National Basic Research Program of China (Grants No. 2012CB927401, No. 2011CB921902, No. 2011CB922200), NSFC (Grants No. 10928408, 10874116, 10904090, 11174199, 11134008), SSTCC (Nos. 10QA1403300, 10JC1407100, 10PJ1405700, 11PJ405200), and the Project of Knowledge Innovation Program (PKIP) of Chinese Academy of Sciences, Grant No. KJCX2.YW.W10. D. Q. acknowledges additional support from Shu Guang project supported by Shanghai Municipal Education Commission and Shanghai Education Development Foundation and from Program for Professor of Special Appointment at Shanghai Institutions of Higher Learning. The theoretical work conducted at University of Utah is supported by US DOE-BES (Grant No. DE-FG02-04ER46148).

*Corresponding author.
fliu@eng.utah.edu
†Corresponding author.
dqian@sjtu.edu.cn
‡Corresponding author.
clgao@sjtu.edu.cn

[1] B. A. Bernevig, T. L. Hughes, and S.C. Zhang, Science **314**, 1757 (2006).
[2] M. König, S. Wiedmann, C. Brüne, A. Roth, H. Buhmann, L. W. Molenkamp, X.L. Qi, and S.C. Zhang, Science **318**, 766 (2007).
[3] L. Fu and C. L. Kane, Phys. Rev. B **76**, 045302 (2007).
[4] D. Hsieh, D. Qian, L. Wray, Y. Xia, Y. S. Hor, R. J. Cava, and M. Z. Hasan, Nature (London) **452**, 970 (2008).
[5] H. J. Zhang, C.X. Liu, X.L. Qi, X. Dai, Z. Fang, and S.C. Zhang, Nature Phys. **5**, 438 (2009).
[6] M. Z. Hasan and C. L. Kane, Rev. Mod. Phys. **82**, 3045 (2010).

[7] Y. L. Chen, J. G. Analytis, J.H. Chu, Z. K. Liu, S.K. Mo, X. L. Qi, H. J. Zhang, D. H. Lu, X. Dai, and Z. Fang, Science **325**, 178 (2009).
[8] X.-L. Qi, R. Li, J. Zang, and S.C. Zhang, Science **323**, 1184 (2009).
[9] L. Fu and C. L. Kane, Phys. Rev. Lett. **100**, 096407 (2008).
[10] R. Yu. W. Zhang, H.J. Zhang, S.C. Zhang, X. Dai, and Z. Fang, Science **329**, 61 (2010).
[11] R. R. Biswas and A. V. Balatsky, Phys. Rev. B **81**, 233405 (2010).
[12] Y. Okada *et al.*, Phys. Rev. Lett. **106**, 206805 (2011).
[13] S. Murakami, Phys. Rev. Lett. **97**, 236805 (2006).
[14] Z. Liu, C.X. Liu, Y.S. Wu, W.H. Duan, F. Liu, and J. Wu, Phys. Rev. Lett. **107**, 136805 (2011).
[15] M. Wada, S. Murakami, F. Freimuth, and G. Bihlmayer, Phys. Rev. B **83**, 121310(R) (2011).
[16] Yu. M. Koroteev, G. Bihlmayer, E. V. Chulkov, and S. Blügel, Phys. Rev. B **77**, 045428 (2008).
[17] T. Hirahara, G. Bihlmayer, Y. Sakamoto, M. Yamada, H. Miyazaki, S.i. Kimura, S. Blügel, and S. Hasegawa1, Phys. Rev. Lett. **107**, 166801 (2011).
[18] L. Miao *et al.* (unpublished).
[19] Y. Y. Li, Y. Y. Li, G. Wang, X. G. Zhu, M. H. Liu, C. Ye, X. Chen, Y. Y. Wang, K. He, L. L. Wang, X. C. Ma, H. J. Zhang, X. Dai, Z. Fang, X. C. Xie, Y. Liu, X. L. Qi, J. F. Jia, S. C. Zhang, and Q. K. Xue, Adv. Mater. **22**, 4002 (2010).
[20] X. Chen, X.C. Ma, K. He, J.F. Jia, and Q.K. Xue, Adv. Mater. **23**, 1162 (2011).
[21] G. Kresse and J. Hafner, Phys. Rev. B **47**, 558 (1993).
[22] D. Yu, E. M. Lupton, M. Liu, W. Liu, and F. Liu, Nano Res. **1**, 56 (2008).
[23] C. Tao and L. Jiao *et al.*, Nature Phys. **7**, 616 (2011).
[24] K. Lai, W. Kundhikanjana, M. A. Kelly, Z.X. Shen, J. Shabani, and M. Shayegan, Phys. Rev. Lett. **107**, 176809 (2011).
[25] T. Hirahara *et al.*, New J. Phys. **10**, 083038 (2008).
[26] P. Cheng *et al.*, Phys. Rev. Lett. **105**, 076801 (2010).